Figure S4 Injury pattern in various injury models.

(A and B) Tissue section of the DDC liver (3-wk treatment). Immunostaining for CK19 (A, purple) and HE staining (B) are shown. Porphyrin (brown particles) accumulates from around the portal vein. PV, portal vein; CV, central vein. (C) CDE liver (1-wk treatment) immunostained for CK19 (red) and cleaved Caspase3 (green) as well as stained with Hoechst (blue). Autofluorescence is shown in white in the merged image. The peri-portal region is injured. (D) HE staining of the liver harvested 2 d after a single CCl_4 injection. The peri-central region is injured. (E) HE staining of the TAA liver (2-d treatment). The peri-central region is injured. (F) Tissue section of the TAA liver (1-wk treatment). Immunostaining for collagen (red) indicates fibrosis in the peri-central region, and TUNEL assay (green, arrows) indicates some apoptotic cells, presumably reflecting inflammation. Particles with high autofluorescence (shown in white, arrowheads) accumulate around the injured area. Blue shows staining with Hoechst. Scale bars: 100 μm.

Figure S5 Calculation of D_{random}.

In cases where the vectors are uniform in length and evenly oriented to various directions, D_{random} was calculated as a sin function (see also Supplementary Materials and Methods). In this case, the direction of the vector sum is vertical to the tangential plane.

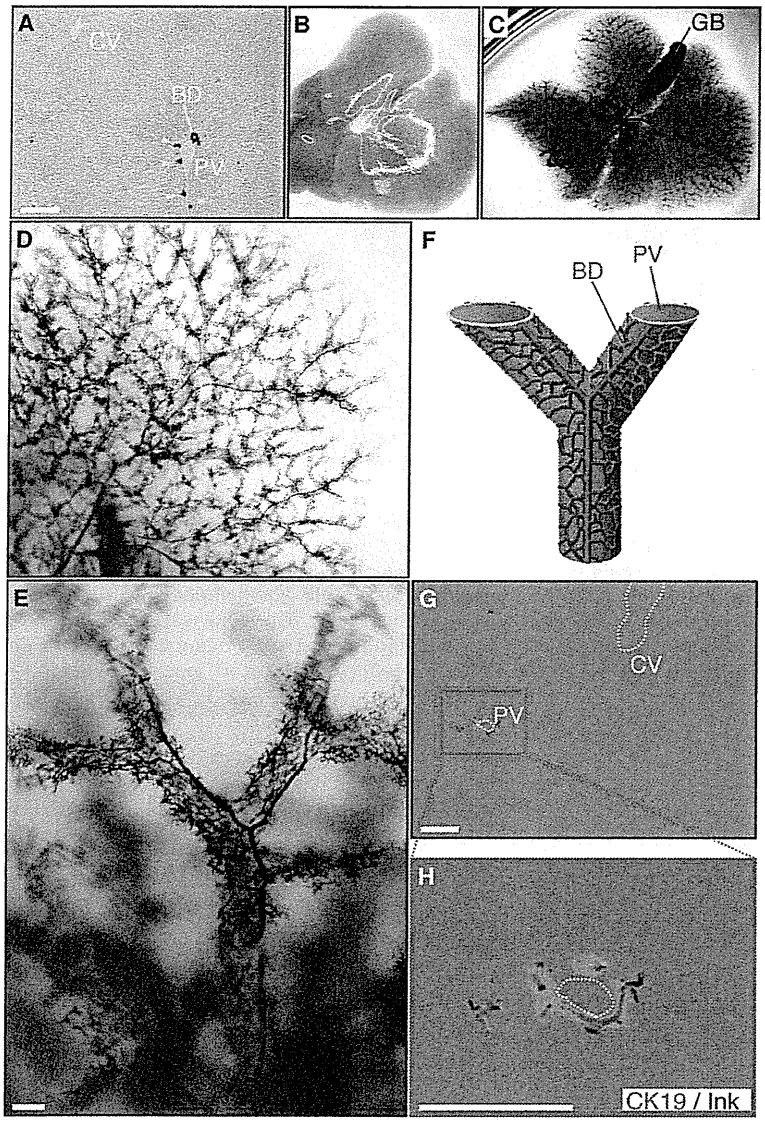

Figure 1 A novel approach for visualizing the fine-scale 3D architecture of the mouse biliary tree. (A) A liver section immunostained with biliary marker CK19. Arrowheads show $CK19^+$ cells without apparent tubular structure. PV, portal vein; CV, central vein; BD, bile duct. (B) Harvested liver without any treatment. (C–E) Architecture of the biliary tree (fine black structure) visualized by using the method developed in this study. GB, gall bladder. (F) Model for the architecture of the biliary tree. The green shows the bile ducts, and the pink shows the portal vein. (G and H) Immunostaining for CK19 (green) on a tissue section of a liver whose biliary tree was filled with ink. Fluorescence image and bright field image are merged. Black ink is colocalized with $CK19^+$ cells. Scale bars: 100 μm in (A, E, G, and H).
137x202mm (300 x 300 DPI)

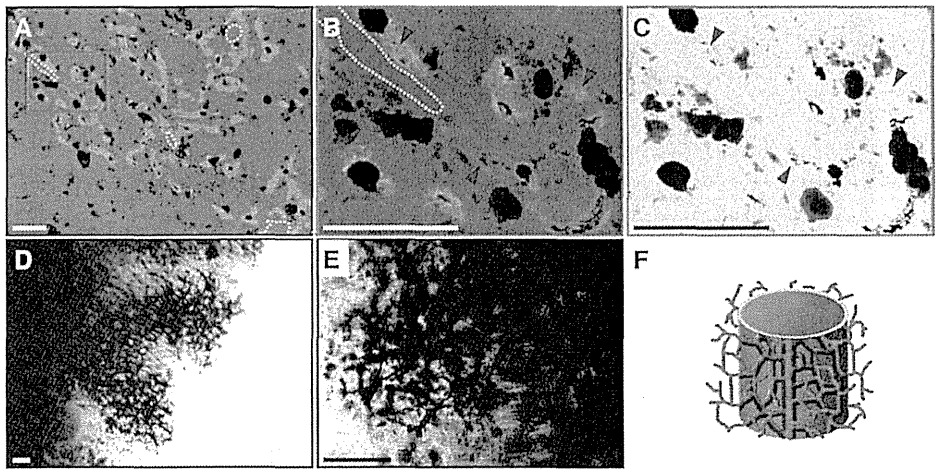

Figure 2 The liver dynamically transforms the biliary tree in response to chronic injury. (A–C) Immunofluorescent staining for CK19 (green) on a section of the DDC-treated liver whose biliary tree was filled with ink. White dashed lines outline the portal vein. (C) The same field as (B) without the fluorescent image. The black ink is colocalized with $CK19^+$ cells (arrowheads). The brown particles are the porphyrin that accumulates along with the toxic injury by DDC. The color tone is adjusted to emphasize the contrast between the ink and the porphyrin (see also Figures S1A, S1C and S1D). (D–F) Architecture of the biliary tree visualized with ink (black) in the DDC-treated liver (D and E) and its schematic model (F). Scale bars: 100 μm in (A–E).
155x77mm (300 x 300 DPI)

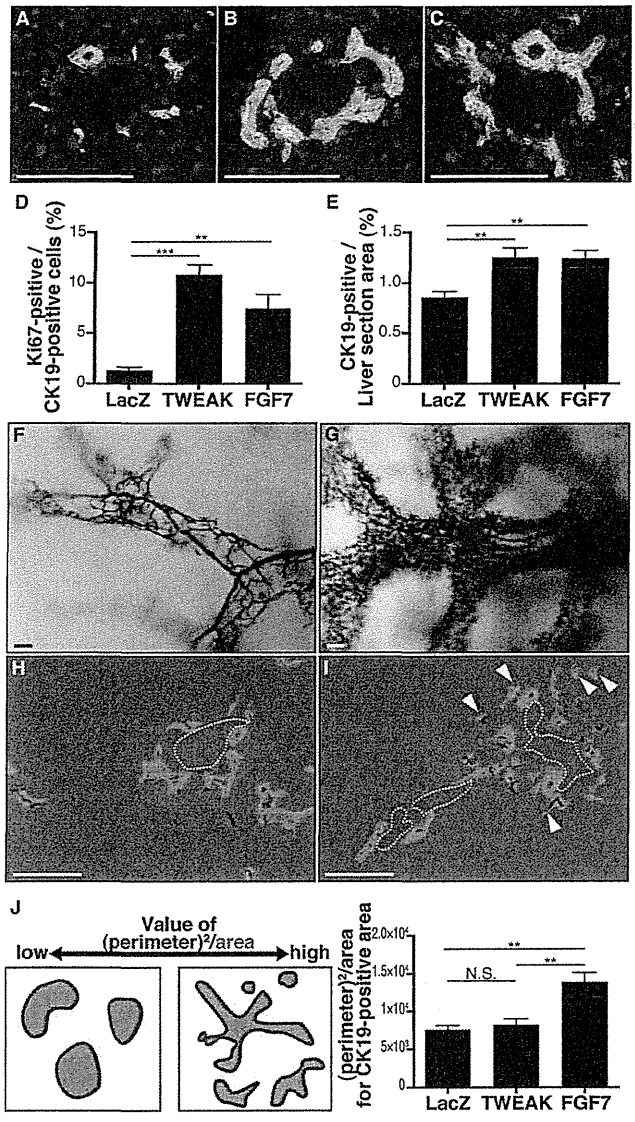

Figure 3 Different effects of FGF7 and TWEAK on the biliary epithelium.
(A–C) Immunofluorescent staining for CK19 (green) and the proliferation marker Ki67 (red) on tissue sections of the livers where LacZ (A), TWEAK (B). or FGF7 (C) was overexpressed. Blue shows nuclei. (D) Quantification of the proliferation of BECs in the liver upon overexpression of LacZ, TWEAK, or FGF7. Percentages of $Ki67^+$ cells in $CK19^+$ cells calculated by cell numbers are shown. (E) Percentages of $CK19^+$ area per the entire liver section area were calculated for the livers where LacZ, TWEAK, or FGF7 was overexpressed. (F and G) Architecture of the biliary tree in the livers upon overexpresson of TWEAK (F) or FGF7 (G). Note that the branches increase intricately in the FGF7-overexpressed liver. (H and I) Immunofluorescent staining for CK19 (green) on the sections of the livers upon overexpression of TWEAK (H) or FGF7 (I), whose biliary tree was filled with ink. White dashed lines outline the portal vein. The black ink is colocalized with $CK19^+$ cells, including those distant from the portal vein in the FGF7 overexpressed liver (arrowheads). (J) The value of $(perimeter)^2$/area was calculated for all the $CK19^+$ regions in the whole section of the livers with LacZ, TWEAK, or FGF7 overexpression. Schematic (left) shows hypothetical area

patterns for low and high values of (perimeter)^2/area. Scale bars: 100 μm. n = 5 mice for each group in (D, E and J). $^{**}P < 0.01$; $^{***}P < 0.001$; N.S., not significant. Error bars represent SEM.
135x243mm (300 x 300 DPI)

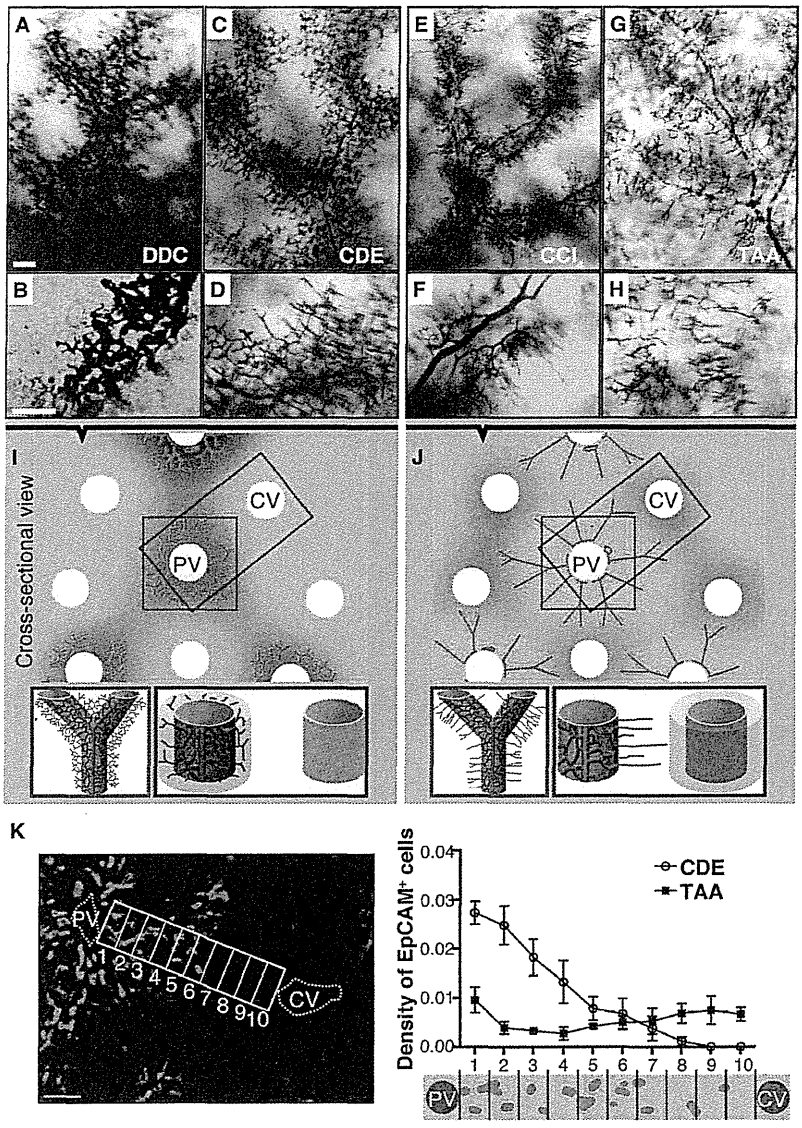

Figure 4 The biliary tree exhibits widely different architectures for various injuries. (A–H) Architecture of the biliary tree in liver injury models caused by DDC (A and B), CDE (C and D), CCl4 (E and F), and TAA (G and H). Scale bars, 100 μm. (I and J) Schematic models for the biliary architectures. Top panels depict a cross-sectional view representing the injury pattern (reddish area) deduced from the histological analyses shown in Figure S4, and the branching pattern of the biliary branches (green) based on the observations shown in the panels A-H. Lower panels show 3D models for the expanded biliary branches around the portal vein (blue box) and in relation to the central vein (purple box; gray zone represents injury area). PV, portal vein; CV, central vein. (I) Biliary branches split intricately around the portal vein; (J) biliary branches are directed to the injured areas. (K) Proportion of biliary marker EpCAM$^+$ area in each zone from the portal vein to the central vein (1 to 10, x-axis) in the CDE and the TAA models were calculated. The left panel shows immunostaining for EpCAM (green) and tissue autofluorescence (magenta) used for identification of PV and CV. Scale bar, 100 μm. Y values were normalized for each mouse so that each graph area correlates with the proportion of total EpCAM$^+$ cells in the whole section. n = 3 mice × 10 fields for

each group. Error bars represent SEM.
158x223mm (300 x 300 DPI)

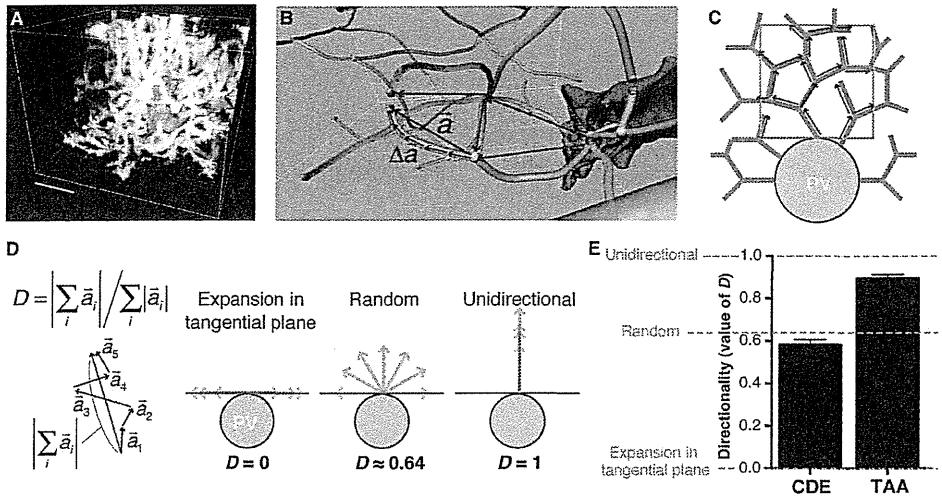

Figure 5 *Directionality of the biliary branches shows different patterns corresponding to injury types.* (A) 3D appearance of the reconstructed biliary branches. White shows the staining for CK19 and pink shows the portal vein (see Supplementary Materials and Methods for information on the reconstruction). Scale bar, 50 μm. (B) 3D image of vector extraction method. Green shows the skeletonized biliary branches. Note that the sum of the minute vectors tracing the branches equals the vector from the starting point to the end. (C) Schematic vector extraction method. Green shows the biliary branches and the orange box represents the region of interest (ROI; see Supplementary Materials and Methods). PV, portal vein. (D) Parameter *D* was calculated for directionality. Simple theoretical values for the parameter *D* in possible distinctive cases are shown. (E) The value of *D* was calculated for the CDE and TAA models. Orange dashed lines show simple theoretical values for each indicated case shown in (D). *n* = 3 mice, total of 17 fields for each group. Error bars represent SEM.
205x110mm (300 x 300 DPI)

Supplementary Materials and Methods

Overexpression of FGF7 and TWEAK in the mouse liver by hydrodynamic tail vein injection

The mouse cDNAs for *Fgf7* and *Tnfsf12* (encoding Tweak) were amplified by PCR with the following primer sets using cDNA prepared from the liver of DDC-treated mice: *Fgf7*, 5'-gaattcgccaccatgcgcaaatggatactgacac-3' and 5'-gcggccgcatgtacacttaggttattgcca-3'; *Tnfsf12*, 5'-cagatctgccaccatggccgcccgtcggagccag-3' and 5'- gcggccgctcagtgaacttgaaagagtcc-3'. The amplified fragments were cloned into the pGEM-T Easy vector (Promega, USA), sequence-verified, and then subcloned into the expression vector pLIVE (Mirus, USA). pLIVE-Fgf7 or pLIVE-Tweak (20 μg) was delivered into C57BL/6J mice using the hydrodynamic tail vein injection procedure (18, 19) and the TransIT-EE Hydrodynamic Delivery Solution (Mirus, USA). pLIVE-LacZ (20 μg) was used as a control. 12-14 days after injection, the mice were subjected to the biliary tree analysis by the ink injection protocol described below.

Analyses with tissue sections

Dissected livers were directly embedded in Tissue-Tek O.C.T. Compound (4583; Sakura Finetek USA, Inc.), and snap frozen. Frozen sections (10 μm) of the liver were prepared using a HM525 cryostat (Microm International) and placed on Aminopropyltriethoxysilane-coated glass slides (Matsunami Glass). Fixation was performed with acetone or 4% Paraformaldehyde after sectioning or with Zamboni's Fixative before sectioning. After blocking in 5% skim milk/PBS, the samples were incubated with primary antibodies and then with fluorescence-conjugated secondary antibodies. Nuclei were counterstained with Hoechst 33342 (Sigma). Liver sections were imaged with a fluorescence (Axio Observer.Z1; Zeiss) or confocal microscope (Fluoview FV1000; Olympus). Fluorescence image and bright field image were merged for the immunostaining on sections of liver whose biliary tree was filled with ink.

For immunostaining of 200-μm sections, the samples were treated in 2-ml tubes for incubation with antibodies and in 50-ml tubes for washing with PBS, and not placed on the slides until just before imaging with the confocal microscope. After sectioning, these

thick sections were fixed with Zamboni's Fixative and permeabilized in 5% 2-mercaptoethanol (Sigma)/1% Triton X-100/PBS, and the following treatments were similarly performed as with 10-μm sections except that each step was conducted for longer periods: about three overnights for incubation with antibodies and one overnight for each wash step.

Rat monoclonal antibody against mouse EpCAM (used at a dilution of 1:200; 552370) was purchased from BD Bioscience. Rat monoclonal antibody against mouse Ki67 (1:200; 14-5698-82) was purchased from Abcam. Rat anti-mouse CK19 (TROMA-III) antibody was obtained from the Developmental Studies Hybridoma Bank and used at 250 ng/mL. The rabbit anti-mouse CK19 antibody (1:1000–1:2000) was raised as previously described (36). A mixture of rabbit anti-collagen type I antibody (1:100; 2150-1410; AbD Serotec) and rabbit anti-collagen type III antibody (1:300; ab7778; Abcam) was used to detect collagen fibers. A TUNEL assay was performed using the In Situ Apoptosis Detection kit (MK500; TaKaRa) according to the manufacturer's instructions. Autofluorescence of the tissue was acquired using filters for red or green fluorescence and represented in false colors.

Quantitative analyses in tissue sections

For quantitative analyses of the livers overexpressed with LacZ, TWEAK, or FGF7 (Figures 3D, 3E and 3J), a group of 5 mice were analyzed for each treatment. Sections made from the left lobe were used for immunostaining. For Figure 3D, more than 20 fields in each section were randomly selected for analysis. Numbers of $Ki67^+/CK19^+$ cells were counted and percentages of the $Ki67^+$ cell numbers in $CK19^+$ cells were calculated. For Figures 3E and 3J, total $CK19^+$ regions in the whole section were imaged and the area and the perimeter for each region were calculated using In Cell Analyzer 2000 (GE Healthcare). Total section area was also imaged and analyzed based on the signal of nuclear counterstaining by Hoechst 33342.

Imaging with confocal microscopy and 3D reconstruction for 200-μm-thick section analysis

Confocal image stacks were recorded with a confocal microscope using a 60×/1.2 NA water immersion objective (UPLSAPO 60XW; Olympus). Settings used were: 320 ×

320 pixel frame size; 662 nm pixel size; 800-nm z-distances between sections; and a 20 μs/pixel scan speed. Settings for fluorescence detection were adjusted across the acquisition depth using the Bright Z Stack function attached to FV10-ASW (Olympus) software. Acquired image stacks were reconstructed into 3D images using IMARIS (Bitplane), and the intensity was linearly adjusted. For 3D presentation in Figure 5a, Gaussian smoothing (0.662 voxel radius) was performed. We excluded the surfaces of 200 μm thick sections from analysis, because they are prone to be damaged in the sectioning process and may include branches coming from another portal vein outside the given section. A region of interest (ROI) of 120 × 120 × 120 pixel frame size was used for analyses as described below. Biliary branches were skeletonized as filaments using the "Filament Tracer" application attached to IMARIS (Figure 5B). For 3D presentation, portal veins were identified as the negative region for autofluorescence: images of the autofluorescence were reconstructed into 3D, inverted, and surfaces were virtually constructed using the "Surface" function in IMARIS.

Analysis of directionality of the branches with 200-μm sections

The analysis with vector sets allowed our simple analysis to be less affected by complicated elements such as unclear connections among branches and small branches/protrusions. We presumed that each vector is oriented against the direction of the portal vein. To limit the analysis to roughly one side of the portal vein, we focused on a local ROI with a defined size (Figure 5C).

We calculated the parameter for the directionality (D) as follows:

$$D = \frac{\left|\sum_i \vec{a}_i\right|}{\sum_i \left|\vec{a}_i\right|}$$

where $\vec{a}_i$ is every vector in the ROI. As shown in Figure 5D, when the branches randomly spread and only in the tangential plane, D becomes 0, and when the branches are completely unidirectional, D becomes 1. For the case where the branches expand completely in a random manner and branch lengths are uniform, we calculated D_{random} as follows:

$$D_{random} = \frac{\int_0^{\pi/2} \sin\theta d\theta}{\pi/2} \approx 0.64$$

where θ is the angle between each vector and the plane vertical to the vector sum and

is evenly distributed from 0 to $\pi/2$ (Figure S5).

We also calculated the parameter D' as follows:

$$D' = \frac{\left|\sum_i \vec{a}_i\right|}{T}$$

where T is the total filament length in the ROI calculated by IMARIS. In this parameter, the practical filament length was applied instead of the vector length. When we compared D and D' calculated in the CDE and TAA liver, the difference between these two injury models did not change substantially, indicating that the approximation of branches to vectors minimally affects the results (the value of D' was 0.51 ± 0.02 for the CDE model, and was 0.81 ± 0.03 for the TAA model).

Distribution analyses in 2D sections

Tissue sections were immunostained for EpCAM, and zones from the portal vein to the central vein were set as shown in Figure 4K (left panel, 1 to 10). EpCAM-positive areas were applied to the density plot using ImageJ software; the mean density in each zone was calculated, and the total value of all zones from the portal vein to the central vein

was normalized to the value of $EpCAM^+$ area/section area for each sample.

Supplementary References

36. Tanimizu N, Nishikawa M, Saito H, Tsujimura T, Miyajima A. Isolation of hepatoblasts based on the expression of Dlk/Pref-1. J Cell Sci 2003;116:1775-1786.